

# Preparation and characterization of titanium tungstophosphate immobilized on mesoporous silica SBA-15 as a new inorganic composite ion exchanger for the removal of lanthanum from aqueous solution

M. Ahmadi<sup>1</sup> · R. Yavari<sup>2</sup> · A. Y. Faal<sup>1</sup> · H. Aghayan<sup>2</sup>

Received: 28 November 2015 / Published online: 3 March 2016  
© Akadémiai Kiadó, Budapest, Hungary 2016

**Abstract** In this study, a novel inorganic composite ion exchanger based on titanium tungstophosphate (TWP) and mesoporous silica SBA-15 has been synthesized. The synthesized product was characterized by methods and instrumental techniques. The results obtained from X-ray diffraction, N<sub>2</sub> adsorption–desorption and Fourier transform infrared analysis confirm immobilization of TWP on SBA-15. Consequently, the ability of this composite for the adsorption of lanthanum ions from aqueous solution was investigated. Considering the relatively high adsorption capacity of lanthanum onto synthesized composite, this material can be potential candidate for the removal of even trace amount of lanthanum ions from nuclear and other industrial wastewater.

**Keywords** Inorganic composite · Mesoporous silica (SBA-15) · Titanium tungstophosphate · Adsorption · Lanthanum ions

## Introduction

Lanthanum isotopes such as La-139 and La-140 are uranium fission products which found in radioactive wastewater [1]. At the same time, lanthanum as one of the most abundant and reactive elements among rare earth elements due to its unique physical and chemical properties is used

in variety of applications, such as semi-conductor, super alloys, catalysts, special ceramics, and in organic synthesis [2–4]. With the increasing usage of lanthanum in various industries, the possibility of the leak of high concentrations of lanthanum from resulting wastewater to the environment and consequently, entry to the body of human being is very high. Generally, after entering lanthanum ions to the living organisms, the main sites where lanthanum accumulates is bone tissue. Because of its relatively toxic and radioactive properties of produced radioisotopes during nuclear fission of uranium, it can cause cancer with humans [5, 6]. Therefore, endeavors to find efficient methods for lanthanum removal from waste water is always of interest.

Several techniques such as solvent extraction, ion exchange, precipitation, adsorption and so forth have been used for the removal of lanthanum ions from aqueous solution [7–11]. Among them, ion exchangers, especially using inorganic ion exchanger have been interested because of their high adsorption capacity for one or group of elements, radiation, thermal and chemical stability, etc. Inorganic ion exchangers based on polyoxometalates are more attractive in the adsorption and removal of some lanthanide elements from liquid waste media [12–17]. The adsorption of the cations in these materials involves interaction with an oxygen end-atom and a release of protons. The preparation mechanism of these compounds is usually based on a salt formed from the reaction between tri or tetravalent metal ions such as Ce<sup>3+</sup>, Sn<sup>4+</sup>, Zr<sup>4+</sup> or Ti<sup>4+</sup> and heteropoly acids with diverse structures [16]. However, synthesized polyoxometalates known as heteropolyacid salts have very small size particles which results in separation problems even under high speed centrifugation. For address this issue, a solution can be conducted toward supporting them onto the carriers with properties of high surface area and large size particles [18].

✉ R. Yavari  
yavariramin@yahoo.com; ryavari@aeoi.org.ir

<sup>1</sup> Department of Chemistry, Payame Noor University,  
P.O.Box. 37185-311, Qom, Iran

<sup>2</sup> Nuclear Science and Technology Research Institute (NSTRI),  
NFCS, P.O. Box. 11365-8486 Tehran, Iran

More recently, mesoporous silica including MCM-41, MCM-48, SBA-15 or CMI-1 with ordered pore structures with respect to utilizing its acidic features has been universally reported as good solid supports [19–25]. In this regard, SBA-15 with parallel cylindrical pores and axes arranged in a hexagonal unit cell exhibits attractive properties [26]. This material typically has a large pore size (from 10 nm to over 30 nm) and thicker pore walls (between 2 and 6 nm) which provide high hydrothermal stability and is suitable for use in aqueous solution [27, 28]. Therefore, in addition to the above mentioned reason, the privilege of preparation of these materials is taking advantage of the mesostructure and high thermal stability of the SBA-15 as a host accompanied by the superior ion exchange properties of the dispersed polyoxometalates in a single material.

On the other hand, the literature survey reveals that no studies have been reported on the synthesis of polyoxometalates immobilized on SBA-15 for using of them in the adsorption and removal of lanthanum ions from aqueous media. Therefore, the aim of this study was an effort to synthesis and characterization of a novel composite based on titanium tungstophosphate (TWP) which has good affinity toward lanthanum ions and SBA-15, and finally to investigate the adsorption behavior of lanthanum ions onto this composite under various conditions.

## Experimental

### Chemicals

All materials used in this study were of analytical reagent grade. P123 (poly (ethylene oxide)-poly (propylene oxide)-poly (ethylene oxide) (EO20-PO70-EO20), tetraethyl orthosilicate (TEOS 98 %), absolute ethanol (99.98), fuming hydrochloric acid (HCl 37 %), titanium chloride ( $\text{TiCl}_4$ ), tungstophosphoric acid (TWA) and concentrated sulfuric acid ( $\text{H}_2\text{SO}_4$  85 %) were purchased from Merck company.

### Preparation of titanium tungstophosphate

Preparation of bulk TWP Sample was done by adding gradually a 100 mL of  $0.1 \text{ mol L}^{-1}$  aqueous solution of tungstophosphoric acid dropwise with constant stirring to a 100 mL of  $0.1 \text{ mol L}^{-1}$  ethanol solution of  $\text{TiCl}_4$ . This solution was stirred for 24 h and after the formation of precipitate, this material was filtered off, washed with demineralized water, dried in an oven at  $50 \text{ }^\circ\text{C}$  for 24 h and converted to  $\text{H}^+$  form by  $0.1 \text{ mol L}^{-1}$  nitric acid solution.

### Preparation of SBA-15 with fibrous morphology

Synthesis of pristine SBA-15 were performed according to literature method described elsewhere [24, 29]. In this procedure, TEOS as a silica source and P123 as the structure-directing agent was used. In a typical synthesis, 2.0 g of P123 was dissolved in 60 mL of  $2 \text{ mol L}^{-1}$  aqueous HCl and 15 mL of distilled water under stirring, and then 4.4 g TEOS was added dropwise to the solution at room temperature. The mixture was stirred for 24 h at  $40 \text{ }^\circ\text{C}$ , and then the temperature was raised to  $100 \text{ }^\circ\text{C}$  and kept for another 24 h in a Teflon-lined autoclave. Finally the resulting precipitate was filtered, washed carefully with distilled water, air dried, and calcined at  $550 \text{ }^\circ\text{C}$  in air for 5 h to remove the template and obtain the final product SBA-15.

### Incorporation of titanium tungstophosphate on mesoporous silica

Preparation of incorporated titanium tungstophosphate on mesoporous silica, denoted as SBA-15-TWP is performed by using two-steps impregnation method. In the first step, 10 mL of  $0.1 \text{ mol L}^{-1}$  ethanol solution (50 %) of tungstophosphoric acid (WPA) was impregnated by aqueous incipient wetness onto prepared SBA-15, dried at  $100 \text{ }^\circ\text{C}$  overnight and calcined at  $300 \text{ }^\circ\text{C}$  for 3 h. Following this, 10 mL of  $0.45 \text{ mol L}^{-1}$  ethanol solution of titanium tetrachloride was impregnated using ethanol solution wetness technique. The prepared sample was filtered off, washed with ethanol and demineralized water and then dried in an oven at  $50 \text{ }^\circ\text{C}$  for 24 h. After that, the obtained product was immersed in acid ( $\text{HNO}_3$ ,  $0.1 \text{ mol L}^{-1}$ ) to be converted to  $\text{H}^+$  form and finally, it was washed repeatedly with demineralized water and dried in air.

### Characterization of the samples

Characterization of the samples is performed by different conventional techniques. X-ray diffraction studies were made with a Philips X-pert diffractometer (model PW 1130/90) using nickel-filtered  $\text{Cu-K}\alpha$  radiation at 298 K. The study was done between  $4$  and  $75^\circ 2\theta$  values with step size 0.05. SEM images are recorded by Philips XL-300 instrument. Fourier transform infrared (FT-IR) spectra were recorded in transmission mode using a NEXUS 670 FT-IR. The quantitative determination of metal ions was carried out using an inductively coupled plasma-optical emission Spectrometry (ICP-OES) model Varian turbo axial. Thermogravimetric analysis was performed on a thermobalance (PL-STA 1500, PL Thermal Science) from

20 to 700 °C at a heating rate of 10 °C min<sup>-1</sup> and a nitrogen flow of 200 mL min<sup>-1</sup>. N<sub>2</sub> adsorption-desorption isotherms were measured on a Nova Station B instrument at 77 K. Specific surface areas and the pore-size distribution were calculated according to the Brunauer–Emmett–Teller (BET) method, and desorption branch of the isotherm by the Barrett–Joyner–Halenda (BJH) method, respectively.

### Adsorption studies

Batch technique was used to determine the adsorption capacities and percentage of lanthanum ions. For this purpose, 0.1 g of solid sample was suspended in a 20 mL of desired concentration of lanthanum ion solution. The mixture was continuously shaken in shaking bath which was operated at 150 rpm and 25 °C for 24 h. The initial pH of the solution was adjusted at desirable values using negligible volumes of 0.1 mol L<sup>-1</sup> nitric acid and sodium hydroxide solution. At the end of each test, the solid phase was separated from the liquid phase by filtration and the concentration of lanthanum in aqueous solution before and after equilibration was measured by ICP-OES elemental analysis. Also the influence of variables conditions such pH, ionic strength, contact time, concentration of metal ions and temperature of solutions were investigated under these conditions and their related parameter. The adsorption capacities and percentage of lanthanum was calculated by the following Eqs. (1) and (2), respectively.

$$q_e = \frac{(C_0 - C_e)v}{M} \quad (1)$$

$$P = \left(1 - \frac{C_e}{C_0}\right) \times 100\% \quad (2)$$

where  $C_0$  and  $C_e$  are the initial and final concentration of lanthanum ions in mg L<sup>-1</sup>,  $v$  is the volume of the initial solution in L and  $M$  is the mass of the ion exchanger in gram.

## Results and discussion

### TWP incorporated on mesoporous silica

One of the main problems for immobilization of heteropolyacid salts on the support is a selection of suitable method which guarantee the high dispersion of particles on the support without aggregation. Since these types of heteropolyacid salts are not soluble in any solvent, one-step impregnation of reagents is obviously unsuitable because the formed insoluble salt of heteropoly acid cannot directly deposit on the surface or channel of the support.

This is due to the absence of any significant attractive force between salt of heteropoly acid and silanol groups on SBA-15 surface [30]. Thus the immobilization on engineered supports must be done via separately impregnation steps for each precursor. As a result of this procedure, the insoluble particles of heteropoly salt are formed within channels or external or internal surfaces of carriers. In addition, this surface impregnation method may exert better control over the homogeneity of the heteropoly compounds. Therefore in the present study, the procedure of loading was performed by two steps impregnation method.

However, another important factor in these type of immobilization is the priority of impregnation of reagents. Both of them, heteropoly acid and titanium chloride, were examined as the first step. The results of experiments (amount of leaching for each reagent by water in 24 h after loading) showed that heteropoly acid as the first precursor can better interact with silanol groups present at the surface or inter channel of mesoporous silica by acid-base interaction. In fact, the protons migrate from heteropoly acid (as Bronsted acid) on silanol groups (as the base) producing SiOH<sup>2+</sup>, which serves as a counter ion for the (SiOH<sup>2+</sup>) (H<sub>2</sub>PW<sub>12</sub>O<sub>40</sub><sup>-</sup>) polyanion. These interactions ensure a stable and non-physically adsorption pattern for heteropoly acid intercalation within the silica support [31], then the dissolution during the second impregnation is prevented. Based on the results obtained by other researchers, thermal treatment after first impregnation is also important to prevent heteropoly acid on SBA-15 from aggregating into the large particles and dissolution during procedure [30].

### Characterization of samples

Figure 1a, b show the low and wide angle XRD patterns of pure SBA-15, TWP and SBA-15-TWP, respectively. As can be seen, SBA-15 exhibits a single strong peak (100) and two weak peak (110, 200) in low angel region, which can be confirmed on highly ordered two dimensional hexagonal mesoporous structure and order lattice having space group symmetry p6 mm [32]. After TWP intercalation in the SBA-15 channels, all three peaks are still detectable indicating that hexagonal pore structure has not been destroyed and TWP has been well dispersed into mesoporous silica. Also, a slight shift in these peaks from low-angel to higher angle is observed which imply the decrease in d-spacing in the synthesized composite. On the other hand, the relative intensities decrease of the (100), (110), and (200) bands in the pattern suggest that TWP species have occupied the mesoscopic cavities of SBA-15 [33, 34].

In wide angle XRD patterns (Fig. 1b), pure SBA-15 shows a broad band with weak intensity at 2θ value of

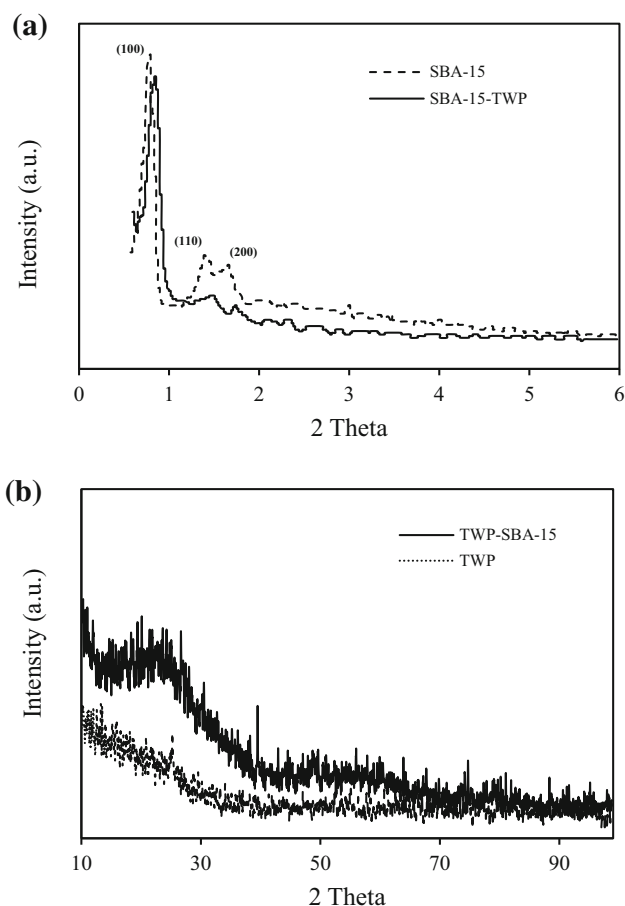


**Fig. 1** **a** Low and **b** wide angel XRD pattern of SBA-15, SBA-15-TWP and TWP

20–30° indicating its amorphous nature. At the same time, the weak intensities of peaks in the X-ray diffraction pattern of TWP suggest that the synthesized polyoxometalate has amorphous structure.

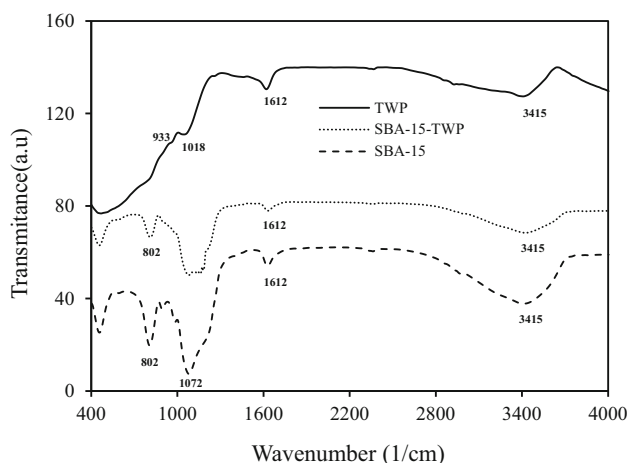


**Fig. 2** IR spectra of SBA-15, SBA-15-TWP and TWP

FT-IR technique as a qualitative method was used to interpret and characterize the structure of synthesized materials. Figure 2 shows the FT-IR spectra of pristine SBA-15, SBA-15-TWP and TWP. As shown for all spectra, the absorption broad and strong band situated between 3000 and 3800  $\text{cm}^{-1}$  with the maximum at 3410  $\text{cm}^{-1}$  and the sharp absorption band at 1612  $\text{cm}^{-1}$  are ascribed to the symmetrical stretching vibration of SiO–H bond in the surface silanol groups [35] and the deformation vibration of free water molecules adsorbed on the materials [33], respectively. In the spectrum of pure SBA-15, Bands corresponding to stretching vibrations of the mesoporous framework (Si–O–Si and Si–O) are detected at 1072 and 802  $\text{cm}^{-1}$ . The bands at 1018 and 933  $\text{cm}^{-1}$  may be assigned to symmetric stretching of the P–O bond and W–O bond in the IR spectrum of TWP sample [36]. After incorporation of TWP on the SBA-15 due to the overlap of P–O and W–O bands with those of Si–O–Si stretching vibration of mesoporous support, the broad band in the range of 900–1200  $\text{cm}^{-1}$  in the composite material was observed. This can be reason of the immobilization of TWP on the SBA-15.

Figure 3 shows SEM images of SBA-15 before (left) and after (right) incorporation of TWP. The formation of SBA-15 with rod morphology and regular hexagonal structure was confirmed by this technique. As can be seen in these figures, the outer diameter of SBA-15 and its composite are less than 50 nm.

Nitrogen adsorption–desorption isotherms of the parent SBA-15 and SBA-15-TWP samples have been shown in Fig. 4. According to the original International Union of Pure and Applied Chemistry (IUPAC) classification [37], pure SBA-15 curve with a sharp inflection capillary condensation step at  $P/P_0 = 0.55$ – $0.85$  and a  $H_1$  type hysteresis loop imitates a type IV isotherm which is commonly associated with the presence of mesoporosity in this structure. In this figure, Nitrogen adsorption–desorption isotherm of SBA-15-TWP sample shows a broadening and the shift in the hysteresis loops toward low relative pressure as well as the decrease in adsorbed nitrogen volume. A reasonable explanation for this observation is that the most of the TWP clusters is introduced into the pores of SBA-15 and caused the partial blockage of mesoporous channels of SBA-15.

The amounts of specific surface area and pore size distribution (including average pore diameter and pore volume) were calculated by obtained  $\text{N}_2$  adsorption/desorption data and using the Brunauer, Emmett, and Teller (BET) and Barrett, Johner, and Halenda (BJH) equations. These physical properties for SBA-15 and SBA-15-TWP are shown in Table 1. The decrease of obtained parameters after loading TWP onto SBA-15 is also due to the occupation of SBA mesoporous by the bulk of TWP. This

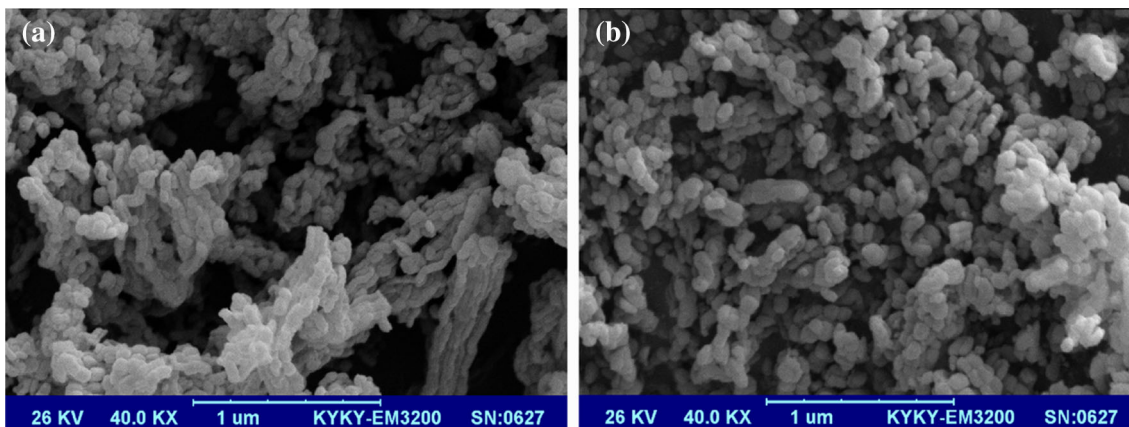


**Fig. 3** SEM image of SBA-15 before (a) and after (b) immobilization of TWP

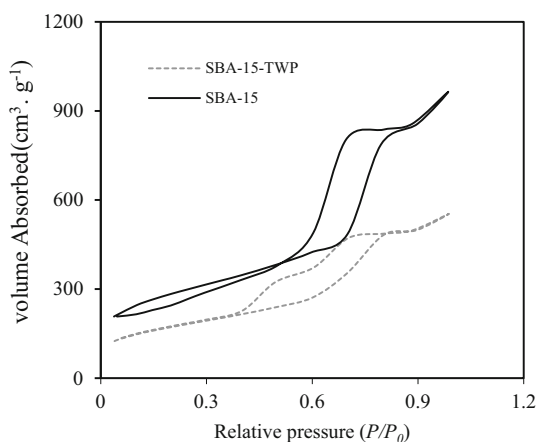


**Fig. 4** N<sub>2</sub> adsorption/desorption isotherms of SBA-15 and SBA-15-TWP

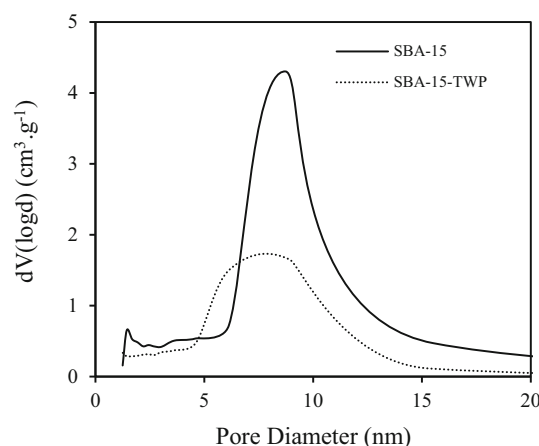


**Fig. 5** Pore size distributions of SBA-15 and SBA-15-TWP

subject was confirmed by investigation the pore-size distribution curves of the samples at Fig. 5. As shown in this figure, there is considerable decrease in pore diameter after loading of TWP. It implies that the TWP are mainly located on the internal and external surface pore of SBA-15, too. The wall thickness for SBA-15 was calculated using the following equation [38]:

$$\text{Wall thickness} = \frac{2d_{100}}{\sqrt{3}} - \text{BJH average pore diameter} \quad (3)$$

The calculations show the value of 25 Å for the SBA-15 and about 32 Å for the SBA-15-TWP. This considerable increase in the thickness of SBA-15-TWP pore wall is

further evidence that the TWP species are located inside the pores of SBA-15.

In order to investigate of the thermal stability, the proportion and decomposition process of material, thermogravimetric (TG) and differential scanning calorimetry (DSC) analysis was used. Figure 6a, b show TGA and DSC profiles of TWP and SBA-15-TWP. As can be observed, the TG curve of TWP shows a continuous loss in weight with total weight loss equal 9.91 % up to 400 °C. The decrease in weight up to this temperature is due to the evaporation of free and structural water molecules that can be supported from DSC endothermic peak at 51 and 120 °C, respectively. The curve of SBA-15-TWP shows

**Table 1** Physical properties (BET surface areas, pore size and pore volume) of SBA-15 and SBA-15-TWP

No.	Samples	BET surface area (m <sup>2</sup> /g)	Pore diameter (nm)	Pore volume (cm <sup>3</sup> /g)
1	SBA-15	1001.979	6.124	1.496
2	SBA-15-TWP	612.050	3.623	0.858



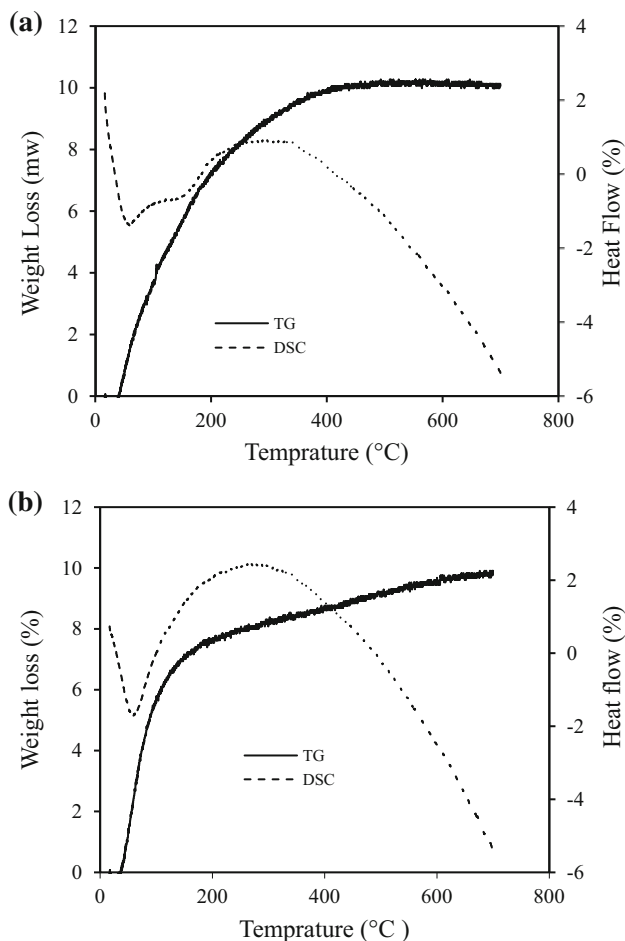


**Fig. 6** TGA (a) and DSC (b) curve of bulk TWP and SBA-15-TWP

similar thermal behavior with the only difference that related to delay and shift to higher temperatures of dehydration process indicating an increase in thermal stability of TWP structures after intercalation within the support. At the same time, both of figures show that TWP and SBA-15-TWP are stable up to 700 °C.

## Adsorption studies

### Adsorption isotherms

From an economical, safety and environmental point of view, the adsorption capacity is an important factor to determine how much adsorbents need for quantitatively sorption of metal ions from a given wastewater solution. Figure 7 shows the adsorption isotherm of lanthanum by SBA-15-TWP at the initial concentration range of 5–300 mg L<sup>-1</sup>. As can be noticed, the adsorption amount of lanthanum on SBA-15-TWP increases with increasing its concentration and then tends to level off as the

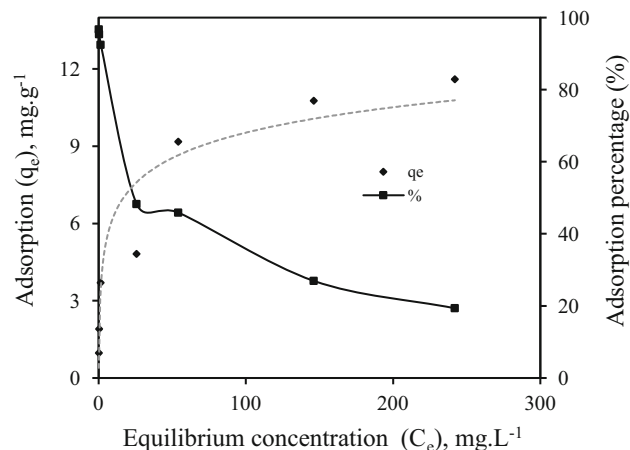


**Fig. 7** Adsorption isotherms of lanthanum ions onto SBA-15-TWP, pH = 6,  $t = 24$  h,  $T = 25$  °C, agitation rate = 150 rpm

adsorbent is saturated. The result implies that the maximum adsorption of 11.6 mg g<sup>-1</sup> obtains for lanthanum adsorption onto our synthesized material.

Most commonly, to describe the relationship between the bulk aqueous phase concentration of adsorbate and the amount adsorbed by unit weight of solid adsorbent at equilibrium condition, adsorption isotherms which are the statistical models are used. Several models have been published to describe experimental data on adsorption isotherms. The Langmuir, Freundlich and Dubinin–Radushkevich (D–R) equations are commonly used for describing adsorption equilibrium for water and wastewater treatment applications. They are characterized by certain constant values, which express the surface properties and affinity of the adsorbent toward metal ions and can also be used to evaluate their adsorption capacities.

The Langmuir adsorption model is valid for monolayer sorption onto completely homogenous surfaces with a finite number of identical sites and uniform adsorption energies [39]. The linear form of the Langmuir isotherm model is given in the following equation;

$$\frac{C_e}{q_e} = \frac{1}{bQ_0} + \frac{C_e}{Q_0} \quad (4)$$

where  $Q_0$  and  $b$  are the characteristic Langmuir parameters.  $Q_0$  is the maximum adsorption capacity that it is the amount of metal to form a complete monolayer and  $b$  is the constant that refers to the bonding energy of adsorption in L mg<sup>-1</sup>. One of the essential parameters of Langmuir equation is the equilibrium parameter or separation factor ( $R_L$ ).  $R_L$  can be calculated by the following equation;

$$R_L = \frac{1}{1 + bC_0} \quad (5)$$

where  $C_0$  (mg/L) is the highest initial solute concentration. The  $R_L$  indicates the type of isotherm to be favorable ( $0 < R_L < 1$ ) or unfavorable ( $R_L > 1$ ).

The Freundlich model assumes that the frequency of sites associated with free energy of adsorption decreases exponentially with increasing free energy and that the energy of adsorption may vary because of heterogeneous real surfaces. The linearized form of the Freundlich equation is given as, [40]:

$$\log q_e = \log k_f + \frac{1}{n} \log c_e \tag{6}$$

where  $k_f$  is the constant related to the adsorption capacity of the adsorbent and  $n$  is the empirical constant related to the intensity of the adsorption and varies with the heterogeneity of the adsorbent.

The Dubinin–Radushkevich (D–R) isotherm model assumes that the surface is heterogeneous. The linear form of the (D–R) equation is given in the following equation [41]:

$$\ln(q_e) = \ln q_{DR} - B_{DR} \epsilon^2 \tag{7}$$

$q_{DR}$  (mmol g<sup>-1</sup>) and  $B_{DR}$  (mol<sup>2</sup> J<sup>-2</sup>) are (D–R) constants related to the adsorption capacity and energy, respectively, and  $\epsilon$  is the Polanyi potential which is expressed by;

$$\epsilon = RT \ln \left( 1 + \frac{1}{C_e} \right) \tag{8}$$

where  $R$  is the gas universal constant (8.314 J mol<sup>-1</sup> k<sup>-1</sup>) and  $T$  is the absolute temperature (K).  $E$  (kJ mol<sup>-1</sup>) is one of the important parameters of (D–R) equation which estimates the type of sorption process (chemical sorption or physical sorption) and can be calculated according to the following equation:

$$E = \frac{1}{\sqrt{2B_{DR}}} \tag{9}$$

If  $1 < E < 8$ , the physical sorption becomes a dominant mechanism. If  $8 < E < 16$ , the chemical sorption becomes a dominant mechanism. The constants of these equations obtained from the slope and intercept of their linear plots and shown in Fig. 8a (Langmuir model), Fig. 8b (Freundlich model) and Fig. 8c (Dubinin–Radushkevich model) are tabulated in Table 2.

Among these sorption models, the best correlation coefficients of the linear regressions ( $R^2$ ) were observed for Langmuir isotherm model. This phenomenon may be due to the homogeneous distribution of active sites on the adsorbent. As can be seen in Table 2, the values of  $R_L$  were between 0 and 1 indicating favorable adsorption. The value of  $n$  is between 1 and 10, indicating again that the sorption is favorable. The values of  $E$  were between 8 and 16

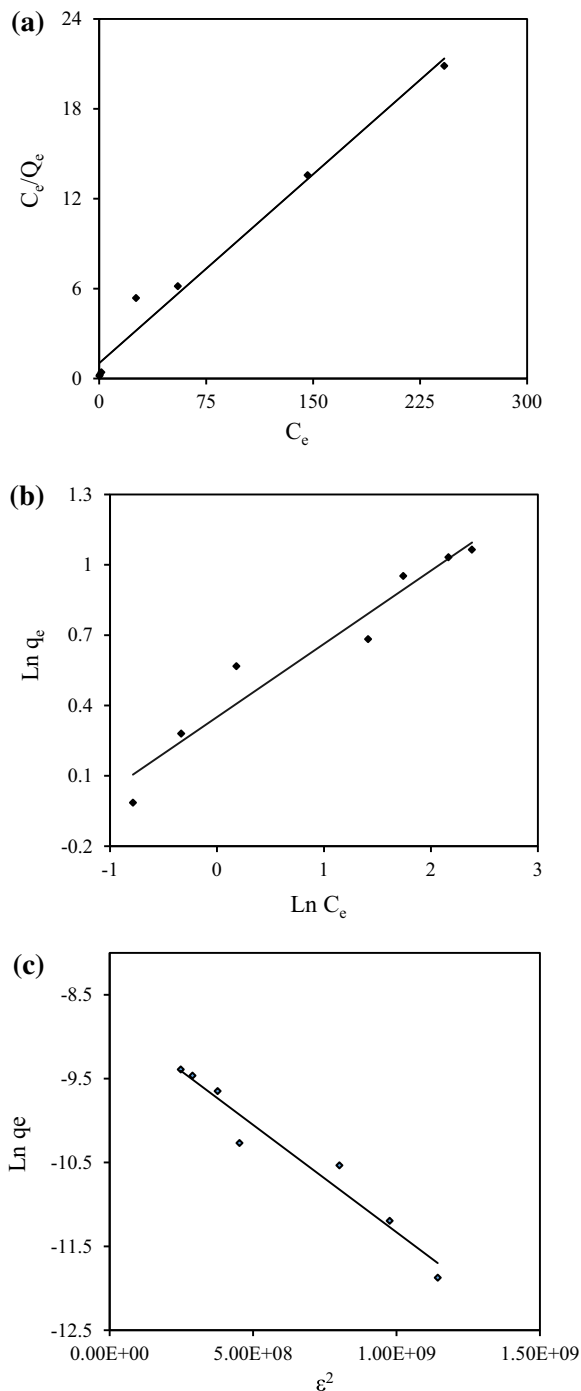


**Fig. 8** a Langmuir, b Freundlich and c Dubinin–Radushkevich linear plots for the adsorption isotherms of lanthanum

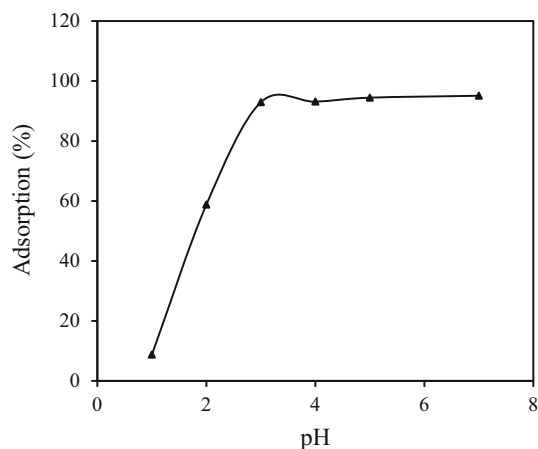
indicating that chemical in addition of physical attraction can be affected on lanthanum ions sorption.

*Effect of pH*

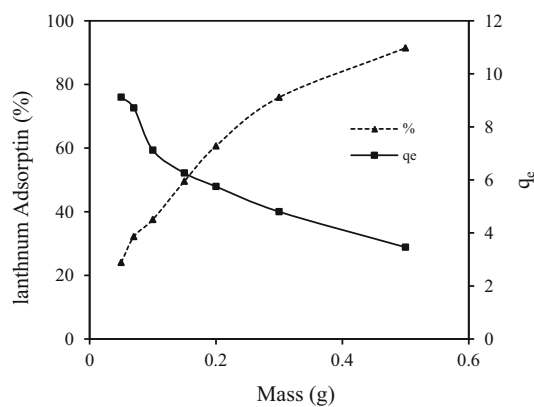
The solution pH value is one of the most important factors which plays the key role in the metal ions adsorption

**Table 2** Langmuir, Freundlich and Dubinin–Radushkevich constants for adsorption of Lanthanum ions on SBA-15-TWP

Metal	Temperature (°C)	Langmuir isotherm			
		$q_m$ (mg/g)	$K_L$ (L/mg)	$R_L$	$R^2$
La	25	11.9047	0.0819	0.039	0.980
		Freundlich isotherm			
		$K_F$ (mg/g)	$n$		$R^2$
		2.241	3.2030		0.942
		Dubinin–Radushkevich isotherm			
		$q_{DR}$ (mmol/g)	$B_{DR}$ (mol <sup>2</sup> /J <sup>2</sup> )	$E$ (kg/mol)	$R^2$
$1.5487 \times 10^{-4}$	$3 \times 10^{-9}$	12.90	0.954		

**Fig. 9** Effect of pH values on the adsorption percentage of lanthanum ions onto SBA-15-TWP,  $t = 24$  h,  $T = 25$  °C, agitation rate = 150 rpm

process from aqueous media. The adsorption percentage of lanthanum at initial concentration of 20 ppm onto SBA-15-TWP as a functional of pH ranging from 1 to 7 is given in Fig. 9. As shown in this figure, the lanthanum uptake increases greatly from pH 1 to 5, reaches a maximum of about 95 % at pH = 5 and does not change considerably at higher pH values. The effects of the solution pH can be related to the competition effect of hydrogen ions with lanthanum ions for the occupation of the adsorbent active binding sites. At very low pH value, where the concentration of the hydrogen ions is high, there is a weak affinity toward SBA-15-TWP on behalf of lanthanum ions. Therefore, the increase in lanthanum removal when the pH increases can be explained on the basis of decrease in competition between proton ions and positively charged metal ions on the adsorbent surface sites. On the other hand, it is well known that the different metal ion species with different degrees of activation can form the metallic cations in aqueous solution as a functional of pH. In the regard of trivalent lanthanides, as a result of hydrolysis, various species of lanthanum such as  $\text{La}(\text{OH})_2^+$ ,  $\text{La}(\text{OH})_3$ ,  $\text{La}(\text{OH})_4^-$  start to form at pH as low as

**Fig. 10** Effect of SBA-15-TWP mass on lanthanum adsorption onto SBA-15-TWP, pH = 6,  $t = 24$  h,  $T = 25$  °C, agitation rate = 150 rpm

6 [27]. At the pH 1–5, the predominant species is  $[\text{La}(\text{H}_2\text{O})_6]^{3+}$  and has higher activity than others. With increasing the pH, the formation possibility of  $\text{La}(\text{OH})_3$  is high making true sorption studies impossible.

#### The effect of adsorbent mass

From the point of view of the economic, safety and environmental, the study of influence of the adsorbent mass on metal ions adsorption from wastewater is an important factor. The effect of synthesized adsorbent mass on the adsorption percentage of lanthanum and the amount of its adsorption ( $q_e$ ) have been depicted in Fig. 10. As shown, with increasing the composite mass, the adsorption percentage of lanthanum increase and its adsorption amount decrease. This can be explained by the fact that the increase in adsorbent mass provides the considerable and available active sites for lanthanum adsorption. On the other hand, due to the saturation of active site of adsorbent in its excess value and limited amount of sorbate, the adsorption amount of lanthanum in the high concentration of composite mass doesn't substantially change.



The effect of ionic strength

For investigation of the effect of sodium nitrate as a criterion of the ionic strength, the different concentrations of sodium nitrate (0.001, 0.01, 0.1, 1 and 2 mol L<sup>-1</sup>) were prepared and added to the solution of lanthanum ions (20 ppm) and 0.1 g of adsorbent. Then, the resulting mixture was stirred for 24 h at optimal pH. Consequently, the obtained adsorption percentage of lanthanum as a functional of sodium nitrate concentration has been depicted in Fig. 11. As can be observed, lanthanum adsorption decreased with increasing ionic strength. Therefore, it implies that there is an intense competitive adsorption between La<sup>3+</sup> and Na<sup>+</sup> ions. This phenomena can be ascribed by the fact that the electrostatically forces cause the adsorption of lanthanum ions on SBA-15-TWP and therefore, the presence of other cations will decrease the adsorption. In other word, it indicates that the adsorption of lanthanum ions takes place through ion exchange interaction [42]. Ionic strength also influences the ionic activity coefficient of lanthanum ions which limit their transfer to adsorbent surfaces and ultimately decrease their adsorption on the active sites of the adsorbent.

Kinetics study

One of the most important characters of the adsorption process and determination of the potential application of an adsorbent is adsorption kinetics which describes the solute adsorption rate governing the residence time of the adsorption reaction. Figure 12 shows the effect of contact time as a functional of lanthanum adsorption percentage from aqueous solution at initial lanthanum concentration of 10 ppm. As shown, in the first 30 min of contact time the

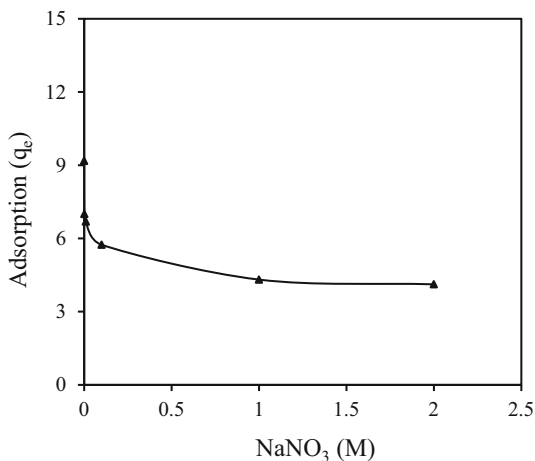


Fig. 11 Effect of ionic strength on the adsorption percentage of lanthanum ions onto SBA-15-TWP, pH = 6, t = 24 h, T = 25 °C, agitation rate = 150 rpm

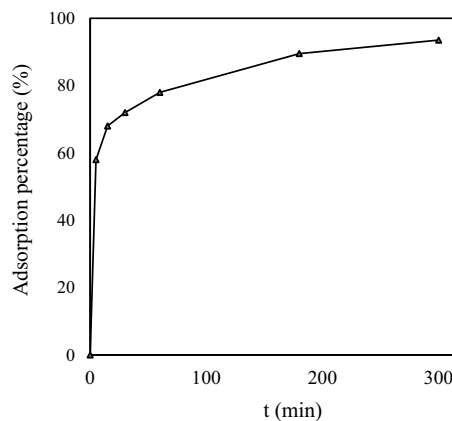


Fig. 12 Effect of shaking time on the adsorption percentage of lanthanum ions onto SBA-15-TWP, pH = 6, t = 24 h, T = 25 °C

adsorption of lanthanum ions increases quickly, and then tends to keep constant after this time. Therefore, the optimal contact time to reach maximum adsorption was obtained 5 h. The initial rapid adsorption can be due to the easy and direct available of lanthanum ions to the external active site of SBA-15-TWP and the next slow step is due to the slow diffusion rate of lanthanum ions into the internal site of adsorbent.

By using the different kinetic models and experimental analysis data, the rate of adsorption of La(III) and potential rate controlling steps such as mass transport and chemical reaction processes can be studied [43]. In the present work, two models of kinetic reaction including pseudo-first-order and pseudo-second-order were used to simulate the kinetic adsorption data of lanthanum on SBA-15-TWP. The integrated and linearized forms of these semi-empirical kinetic model equations are given as follow, respectively [44, 45];

$$\log(q_e - q_t) = \log q_e - \frac{k_1}{2.303} t \tag{10}$$

$$\frac{t}{q_t} = \frac{1}{k_2 q_e^2} + \frac{1}{q_e} t \tag{11}$$

where  $q_e$  and  $q_t$  are, the adsorbed amounts of metal at equilibrium and at time t expressed as mg g<sup>-1</sup>;  $k_1$  and  $k_2$  are the pseudo-first-order and pseudo-second-order constant expressed as min<sup>-1</sup> and g mg<sup>-1</sup> min<sup>-1</sup>, respectively. Figure 13a, b show linear plots of these equations. Linear arrangements are commonly used to check the validity of these models and to obtain the model parameters when the corresponding linear plot is adequate.

The obtained parameters from the slope and intercept of these plots accompanied by their linear regression ( $R^2$ ) are listed in Table 3. As shown, among these kinetic models, the higher correlation coefficient ( $R^2 > 0.997$ ) corresponded to the pseudo-second-order model shows that this model fitted well the kinetic data. In other word, the rate of

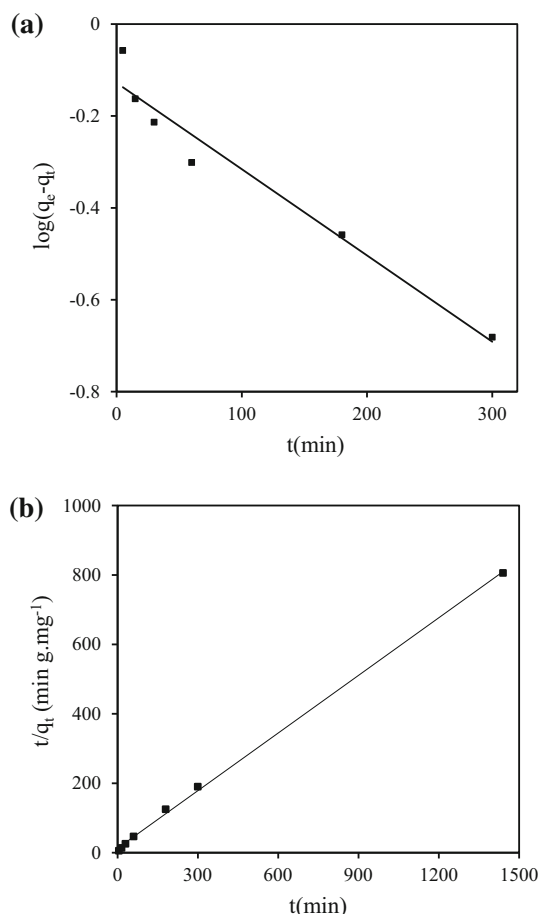


**Fig. 13** **a** Pseudo- first- order and **b** pseudo- second- order linear plots for the adsorption of lanthanum ions onto SBA-15-TWP

La(III) adsorption onto SBA-15-TWP is accurately described by the pseudo-second-order equation that confirms the chemical reaction in addition to physical adsorption of La(III) onto sorbent. When the rate of reaction of an adsorption reaction is controlled by chemical exchange, a pseudo-second-order model can be better adjusted to the experimental kinetic data [46]. On the other hand, as can be seen from Fig. 15, it is clear that pseudo-first-order model isn't suitable model to describe the kinetic profile because of the apparent lack of the linear behavior.

#### Intraparticle diffusion model

To further process the kinetic data and evaluate the extent to which diffusion participates in the sorption process, the

Weber–Morris intraparticle diffusion model was then used [47]. The intraparticle diffusion model assumes that the sorption/desorption mass transfer process can be described by the radial diffusive penetration of chemicals into and out of porous soil particles [48]. by three consecutive steps [27]:

- (i) The transport of sorbate from bulk solution to outer surface of the sorbent, known as external (or) film diffusion.
- (ii) Internal diffusion, the transport of sorbate from the particles surface into interior sites.
- (iii) The sorption of the solute particles from the active sites into the interior surface of the pores.

The Weber–Morris intraparticle diffusion model is described by the following rate equation;

$$q_t = k_d t^{1/2} + c \quad (12)$$

where  $q_t$  is the adsorption capacity at time  $t$  (min) in  $\text{mg g}^{-1}$ ,  $k_d$  is the diffusion rate constant in  $\text{mg g}^{-1} \text{min}^{-1/2}$  and  $c$  is the intercept at the ordinate in  $\text{mg g}^{-1}$ .

The nature of the rate limiting step which is controlled by the slowest of the adsorption process can be determined from the properties of the solute and sorbent. Figure 14 presents plots of  $q_t$  versus  $t^{1/2}$  for various stirring rate and initial lanthanum concentration of 10 ppm whereas the result of the corresponding linear regression analysis has been given in Table 4. As can be seen from Fig. 14, in the range of the studied adsorption, the plots of  $q_t$  versus  $t^{1/2}$  give straight lines consisting of two portions: the first portion occurs in the  $t^{1/2}$  region up to about  $5.47 \text{ min}^{1/2}$  at 200 rpm while the second one corresponds to higher  $t^{1/2}$  values. The sharper slope in the first portion can be assigned to the diffusion of lanthanum ions through the solution to the external surface of the adsorbent known as the boundary layer (film) diffusion. The second portion reflected a gradual adsorption stage is characterized by the intra-particle diffusion of metal ions into mesoporous channels and cavities. The slope of each linear portion indicates the rate of the corresponding adsorption. Therefore, a lower slope describing a slower adsorption process is a rate limiting step [27]. As a result, as shown in Fig. 14, the rate limiting step relates to the second portion which has lower slope. In other word, it implies that the film diffusion proceeds faster than the intraparticle diffusion in the adsorption process. Also, to better identify the effect of

**Table 3** The obtained kinetic parameters using Pseudo-first-order and Pseudo-second-order models

Concentration (mg/L)	$q_e^{\text{exp}}$ (mg/g)	Pseudo -first-order			Pseudo -second-order		
		$k_1$ (1/min)	$q_{e1}$ (mg/g)	$R^2$	$k_2$ (g/mg min)	$q_{e2}$ (mg/g)	$R^2$
10	1.78	0.00435	0.744	0.956	0.649	1.59	0.997

stirring rate on the adsorption process, experiments were performed to determine adsorption capacity at various stirring rate. The obtained results are also tabulated in Table 4. As can be seen from this table, by increasing the stirring rate, a decrease and increase effects in film diffusion and an intraparticle diffusion, respectively, can be caused. For example, by using 50 rpm in our experiments, the process occurs by film diffusion until 60 min of shaking time while by increasing stirring rate up to 200 rpm, the process occurs by film diffusion until 30 min. This phenomenon could be explain by the fact that, the increasing in stirring rate give rise to a decrease in film thickness and consequently decrease boundary layer diffusion resistance.

*Desorption studies*

The applicability of adsorbents depends on both their adsorption capacity and desorption property. As a matter of fact, the desorption process not only allows the recovery of precious adsorbed metal ions from wastewater but also significantly reduce the overall cost for adsorbent through its regeneration.

Desorption of adsorbed lanthanum ions from adsorbent was evaluated by HNO<sub>3</sub> acid solution. The reusability of the adsorbent was measured by repeating the metal ion adsorption–desorption cycle 4 times in the same adsorbent.

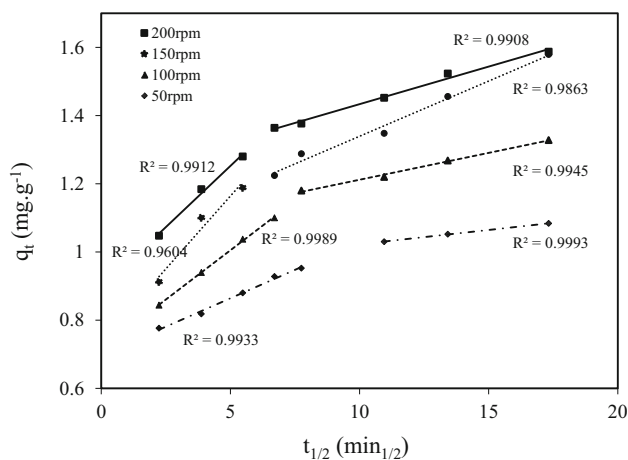


**Fig. 14** Intraparticle diffusion kinetic linear plots for the adsorption of lanthanum ions onto SBA-15-TWP

**Table 4** Rate constants for the Weber- Morris model in adsorption of Lanthanum ions on SBA-15-TWP

Concentration (mg/L)	Stirring rate	Weber–Morris model parameters		
		<i>k<sub>d</sub></i> (mg/g min <sup>1/2</sup> )	<i>C</i> (mg/g)	<i>R</i> <sup>2</sup>
10	50	0.0122	0.826	0.425
	100	0.0273	0.881	0.922
	150	0.0304	1.051	0.997
	200	0.0191	1.220	0.964

The measured adsorption capacity of the adsorbent after four cycles indicates a loss in the adsorption capacity of 8.2 % lanthanum ions compared to the initial cycle, which implies a good regeneration properties of the adsorbent and reversibility of the adsorption process. From these results, it can be conclude that the adsorbent can be used repeatedly for the removal of lanthanum ions from aqueous solution.

*Adsorption thermodynamics*

The effect of temperature on the adsorption of lanthanum ions has been studied in the range of 303–343 K (keeping all the other parameters constant at their optimum value) to evaluate thermodynamic criteria by calculating the Gibbs free energy ( $\Delta G^\circ$ ) by the following equation:

$$\Delta G^\circ = \Delta H^\circ - T\Delta S^\circ \tag{13}$$

$$\ln k_d = \frac{\Delta S^\circ}{R} - \frac{\Delta H^\circ}{RT} \tag{14}$$

where the  $\Delta G^\circ$  is the change in Gibbs free energy in J mol<sup>-1</sup>,  $\Delta H^\circ$  is the change in the enthalpy in J mol<sup>-1</sup>,  $\Delta S^\circ$  is the change in the entropy in J mol<sup>-1</sup> k, *T* is the temperature in *K* and *R* is the universal gas constant (8.314 J mol<sup>-1</sup> k). Also, the values of  $\Delta H^\circ$  and  $\Delta S^\circ$  are obtained from the slope and intercept of  $\ln k_d$  versus  $1/T$  plots. The distribution coefficient (*k<sub>d</sub>*) is calculated from the following formula [49],

$$k_d = \frac{C_0 - C_e}{C_e} \times \frac{V}{W} \tag{15}$$

where *C*<sub>0</sub> and *C*<sub>*e*</sub> are the initial and final concentration (ppm) of lanthanum ions in the solution phase, respectively, *V* is volume of initial solution in mL, and *W* is the dry mass of the adsorbent in g. Figure 15 shows the effect of temperature on the lanthanum adsorption onto SBA-15-TWP by linear plots of  $\ln k_d$  vs.  $1/T$ . From the slop and intercept of this linear graph,  $\Delta H^\circ$  and  $\Delta S^\circ$  were obtained and consequently, the relative parameters and the correlation coefficient of the linear regressions (*R*<sup>2</sup>) calculated from Eqs. (13–15) are listed in Table 5.

The results show that the adsorption of lanthanum ions is favored by increasing temperature. The negative  $\Delta G^\circ$  values show that, the lanthanum adsorption occurs

spontaneously and the spontaneity. Also, the positive values of  $\Delta H^\circ$  and value increase of  $k_d$  with increasing temperature is consistent with an endothermic adsorption process that is favored by an increase in temperature. The positive  $\Delta S^\circ$  values implies that a system become more disordered. In other word, it indicates that with the adsorption of one La (III) ion from solution, three  $H^+$  ions is liberated from adsorbent.

#### Investigation of some metal ions adsorption

Also, the distribution coefficients ( $K_d$ ) is an important parameter to investigate the adsorption behavior of different ions on an adsorbent and estimate the efficiency of an adsorbent in the separation of cations and anions. Table 6 shows the  $K_d$  values of some metal ions (which is usually found in the presence of lanthanum) onto SBA-15-TWP by using batch technique in the optimum condition of lanthanum adsorption. The obtained results show that lanthanum and samarium ions are more strongly adsorbed than other studied metal ions while other metal ions such as sodium, potassium, cobalt, zinc, dysprosium, nickel, copper and iron has low or relatively low  $K_d$  values indicating the low affinity toward these metal ions behalf of SBA-15-TWP. Therefore, we can claim that SBA-15-TWP can be used for selective removal and separation of lanthanum ions from mentioned metal ions in aqueous solution.

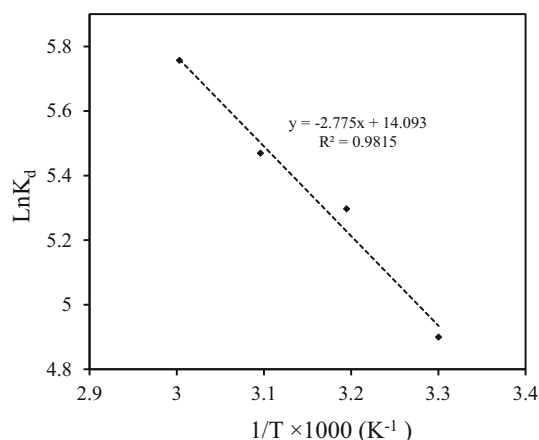


**Fig. 15** Effect of temperature on adsorption of lanthanum ions onto SBA-15-TWP

**Table 5** Thermodynamics parameters of Lanthanum ions on SBA-15-TWP at different temperature in Kelvin

$C_0$ (100 mg/L)	$T$ (K)	$\Delta G^\circ$ (kJ/mol)	$\Delta H^\circ$ (kJ/mol)	$\Delta S^\circ$ (kJ/mol)	$R^2$
La	303	-12.381	23.07	117	0.981
	313	-13.551			
	323	-14.721			
	333	-15.891			

## Conclusion

In this study, immobilization of TWP on mesoporous silica SBA-15 as a novel inorganic composite ion exchanger was performed via efficient and easy two separately wetness impregnation method. The characterization of the composite by FT-IR,  $N_2$  adsorption–desorption isotherms and XRD analyses confirm this successful immobilization. SEM image of this composite showed that the morphology of synthesized material is rod and regular hexagonal structure. Also, considering the result obtained by  $N_2$  adsorption–desorption analysis, the presence of mesoporosity in the structure of the composite is confirmed. The surface area and pore size decrease upon loading and the mesoporous structure of the sample is maintained, as demonstrated by small-angle XRD and  $N_2$  adsorption–desorption data. The TGA and DSC curve of composite show that the prepared material can be used up to 700 °C.

The efficiency of composite for the adsorption of lanthanum ions from aqueous solution was investigated using batch adsorption technique under different experimental conditions. The results show that the uptake of lanthanum was dependent on pH, ionic strength of solution, shaking time, adsorbent mass, metal ion concentration and temperature. The optimum pH for the maximum adsorption of lanthanum was 5.0 and the kinetics analysis revealed that the overall adsorption process was successfully fitted with the pseudo-second-order kinetic model which indicates that

**Table 6**  $K_d$  values of some metal ions on SBA-15-TWP

Metal ions	$K_d$ values (mg g <sup>-1</sup> )
Na	N.A.
K	N.A.
Co	21
Ni	N.A.
Cu	35
Zn	10
La	427
Sm	500
Dy	53
Nd	170
Fe	16

N.A negligible adsorption

the adsorption involves chemical reaction in addition to physical adsorption. The effect of ionic strength and pH indicated that ion exchange mechanism is involved in the adsorption of lanthanum. Among various isotherm models, the Langmuir isotherm model established a strong correlation coefficient with the experimental data which indicate that the surface is homogeneous and the adsorption is monolayer. The data resulting the investigation of the effect of temperature results revealed that the adsorption of lanthanum ions onto adsorbent is dependent on temperature. The positive values of  $\Delta H$  show that the sorption process is endothermic. Also, with increasing temperature, the obtained negative values for  $\Delta G$  confirm better sorption at higher temperatures and indicate that the sorption of ions onto the adsorbent is spontaneous. The investigation of adsorption behavior of some metal ions show that SBA-15-TWP has high affinity toward lanthanum and dysprosium ions.

Based on the results presented in this paper, it is apparent that this method can be extended to prepare the other polyoxometalate–mesoporous silica composites. Also, the high adsorption percentage of lanthanum onto SBA-15-TWP ( $\approx 95\%$ ) in comparison with SBA-15 (11%) in the obtained optimum conditions show that the synthesized composite can be used successfully for the removal of even trace amount of lanthanum ions from nuclear and other industrial wastewater.

## References

- Vasylyeva HV, Strelko VV, Patrylyak SM, Yakovlyev NN, Pylypchenkob VA, Khimich IV (2005) Radiochemical studies of state of lanthanum microamounts in water solution. *J Mol Liq* 118:41–44
- Tadjarodi A, Jalalat V, Zare-Dorabei R (2014) Adsorption of La(III) in aqueous systems by *N*-(2-hydroxyethyl) salicylaldehyde-functionalized mesoporous silica. *Mater Res Bull* 61:113–119
- Kondo K, Kamio E (2002) Separation of rare earth metals with a polymeric microcapsule membrane. *Desalination* 144:249–254
- Vijayaraghavan K, Mahadevan A, Man Joshi U, Balasubramanian R (2009) An examination of the uptake of lanthanum from aqueous solution by crab shell particles. *Chem Eng J* 152:116–121
- Chu HY, Zhu JG, Xie ZB, Zeng Q, Li ZG, Cao ZH (2003) Availability and toxicity of exogenous lanthanum in a haplic acrisols. *Geoderma* 115:121–128
- Huang J, Zhang TL, Xu SJ, Li RC, Wang K, Zhang J, Xie YN (2006) Effects of lanthanum on composition, crystal size, and lattice structure of femur bone mineral of Wistar rat. *Calcif Tissue Int* 78:241–247
- Dongbei W, Yanhong S, Qigang W (2013) Adsorption of lanthanum(III) from aqueous solution using 2-ethylhexyl phosphonic acid mono-2-ethylhexyl ester-grafted magnetic silica nanocomposites. *J Hazard Mater* 260:409–419
- Acharya S, Mishra S, Misra PK (2015) Studies on extraction and separation of La(III) with DEHPA and PC88A in petrofin. *Hydrometallurgy* 156:12–16
- Xie F, Zhang TA, Dreisinger D, Doyle F (2014) A critical review on solvent extraction of rare earths from aqueous solutions. *Miner Eng* 56:10–28
- Zhang F, Wu W, Xue B, Zeng W (2014) Synergistic extraction and separation of lanthanum(III) and cerium(III) using a mixture of 2-ethylhexylphosphonicmono-2-ethylhexyl ester and di-2-ethylhexyl phosphoric acid in the presence of two complexing agents containing lactic acid and citric acid. *Hydrometallurgy* 149:238–243
- Ganjali MR, Daftari Rezapour AM, Puorsaberi T, Haghgoo S (2003) Gliclazide as novel carrier in construction of PVC-based La(III)-selective membrane sensor. *Talanta* 59:613–619
- Li Z, Song-dong D, Tang Y, Guang-Can Z (2009) Adsorption behavior of rare earth elements using polyethylene glycol (phosphomolybdate and tungstate) heteropoly acid sorbent in nitric solution. *Hydrometallurgy* 99:109–114
- Nabi SA, Mumtaz Khan A (2006) Synthesis, ion exchange properties and analytical applications of stannic silicomolybdate: effect of temperature on distribution coefficients of metal ions. *React Funct Polym* 66:495–508
- Nabi SA, Shalla AH, Mumtaz Khan A, Ganie SA (2007) Synthesis, characterization and analytical applications of titanium(IV) molybdosilicate: a cation ion-exchanger. *Colloids Surf A* 302:241–250
- Marageh MG, Waqif-Husain S, Khanchi AR (1999) Sorption of radionuclides on cerium(V) molybdophosphate ion exchanger. *J Radioanal Nucl Chem* 241(1):139–143
- Yavari R, Ahmadi SJ, Huang YD, Khanchi AR, Bagheri G, He JM (2009) Synthesis, characterization and analytical application of a new inorganic cation exchanger—Titanium(IV) molybdophosphate. *Talanta* 77:1179–1184
- Yavari R, Ahmadi SJ, Huang YD, Khanchi AR, Bagheri G (2008) Synthesis, ion exchange properties, and applications of amorphous cerium(III) tungstosilicate. *Sep Sci Technol* 15:3920–3935
- Saemin C, Yong W, Zimin N, Jun L (2000) Cs-substituted tungstophosphoric acid salt supported on mesoporous silica. *Catal Today* 55:117–124
- Parida KM, Rana S, Mallick S, Rath D (2010) Cesium salts of heteropoly acid immobilized mesoporous silica: an efficient catalyst for acylation of anisole. *J Colloid Interface Sci* 350:132–139
- Wei J, Yue Q, Sun Z, Deng Y (2012) Synthesis of dual-mesoporous silica using non-ionic diblock copolymer and cationic surfactant as co-templates. *Angew Chem Int Ed* 51:6149–6153
- Wei J, Wang H, Deng Y, Sun Z, Shi L, Tu B, Luqman M, Zhao D (2012) Solvent evaporation induced aggregating assembly approach to three-dimensional ordered mesoporous silica with ultralarge accessible mesopores. *J Am Chem Soc* 133:20369–20377
- Zhang J, Deng Y, Wei J, Sun Z, Gu D, Bongard H, Liu C, Wu H, Tu B, Schuth F, Zhao D (2009) Design of amphiphilic ABC triblock copolymer for templating synthesis of large-pore ordered mesoporous carbons with tunable pore wall thickness. *Chem Mater* 21:3996–4005
- Deng Y, Liu C, Gu D, Yu T, Tu B, Zhao D (2008) Thick wall mesoporous carbons with a large pore structure templated from a weakly hydrophobic PEO–PMMA diblock copolymer. *J Mater Chem* 18:91–97
- Aghayan H, Khanchi AR, Mahjoub AR (2013) Synthesis and characterization of cesium molybdo vanado phosphate immobilized on platelet SBA-15: an efficient inorganic composite ion-exchanger for gadolinium ion sorption. *Appl Surf Sci* 274:7–14
- Yixiang B, Yan X, Du W, Xie X, Pan Z, Zhou J, Li L (2015) Application of amine-functionalized MCM-41 modified ultrafiltration membrane to remove chromium(VI) and copper (II). *Chem Eng J* 281:460–467



26. Guo W, Chen R, Liu Y, Meng M, Meng X, Hu Z, Song Z (2013) Preparation of ion-imprinted mesoporous silica SBA-15 functionalized with triglycine for selective adsorption of Co(II). *Colloids Surf A* 436:693–703
27. Aghayan H, Khanchi AR, Mahjoub AR (2013) Samarium and dysprosium removal using 11-molybdo-vanadophosphoric acid supported on Zr modified mesoporous silica SBA-15. *Chem Eng J* 225:509–519
28. Shih-Yuan C, Chih-Yuan T, Wei-Tsung C, Jey-Jau LA (2008) Facile route to synthesizing functionalized mesoporous SBA-15 materials with platelet morphology and short Mesochannels. *Chem Mater* 20:3906–3916
29. Zhao DY, Huo QS, Feng JL, Chmelka BF, Stucky GD (1998) Nonionic triblock and star diblock copolymer and oligomeric surfactant syntheses of highly ordered, hydrothermally stable, mesoporous silica structures. *J Am Chem Soc* 120:6024–6036
30. Zhu Z, Yang W (2009) Preparation, characterization and shape-selective catalysis of supported heteropoly acid salts  $K_2.5H_{0.5}PW_{12}O_{40}$ ,  $(NH_4)_{2.5}H_{0.5}PW_{12}O_{40}$  and  $Ce_{0.83}H_{0.5}PW_{12}O_{40}$  on MCM-41 mesoporous silica. *J Phys Chem C* 113:17025–17031
31. Lefebvre F (1992)  $^{31}P$  MAS NMR study of  $H_3PW_{12}O_{40}$  supported on silica formation of  $(SiOH_2^+)(H_2PW_{20}O_{40}^-)$ . *J Chem Soc* 10:756–757
32. Karimi Z, Mahjoub AR, Harati SM (2011) Polyoxometalate-based hybrid mesostructured catalysts for green epoxidation of olefins. *Inorg Chim Acta* 376:1–9
33. Chamack M, Mahjoub AR, Aghayan H (2015) Catalytic performance of vanadium-substituted molybdophosphoric acid supported on zirconium modified mesoporous silica in oxidative desulfurization. *Chem Eng Res Des* 94:565–572
34. Dragoi B, Dumitriu E, Guimon C, Auroux A (2009) Acidic and adsorptive properties of SBA-15 modified by aluminum incorporation. *Microporous Mesoporous Mater* 121:7–17
35. Guo W, Chen R, Liu Y, Meng M, Meng X, Hu Z, Song Z (2013) Preparation of ion-imprinted mesoporous silica SBA-15 functionalized with triglycine for selective adsorption of Co(II) *Colloids Surf A* 436:693–703
36. Pechkovskii VV, Melnikova RY, Dzyuba ED (1985) Atlas of infrared spectra of phosphates, orthophosphate. Nauka, Moscow
37. Sing K, Everett D, Haul R, Moscou L, Pierotti R, Rouquerol J, Siemieniowska T (1985) Reporting physisorption data for gas/solid systems with special reference to the determination of surface area and porosity. *Pure Appl Chem* 57:603–619
38. Zhao D, Feng J, Huo Q, Melosh N, Fredrickson GH, Hmelka BF, Stucky GD (1998) Study, triblock copolymer syntheses of mesoporous silica with periodic 50–300 angstrom pores. *Science* 279:548–552
39. Asadollahi N, Yavari R, Ghanadzadeh H (2015) Preparation, characterization and analytical application of stannic molybdophosphate immobilized on multiwalled carbon nanotubes as a new adsorbent for the removal of strontium from wastewater. *J Radioanal Nucl Chem* 303:2445–2455
40. Gunten UV (2003) Ozonation of drinking water: Part I. Oxidation kinetics and product formation. *Water Res* 37:1443–1467
41. Dogan M, Alkan M (2003) Removal of methyl violet from aqueous solution by perlite. *J Colloid Interface Sci* 267:32–41
42. Zhao DL, Feng SJ, Chen CL, Chen SH, Xu D, Wang XK (2008) Adsorption of thorium(IV) on MX-80 bentonite: effect of pH, ionic strength and temperature. *Appl Clay Sci* 41:17–23
43. Velickovic Z, Vukovic GD, Marinkovic AD, Moldovan MS, Peric-Grujic AA, Uskokovic PS, Ristic M (2012) Adsorption of arsenate on iron(III) oxide coated ethylenediamine functionalized multiwall carbon nanotubes. *Chem Eng J* 181–182:174–181
44. Ho Y (2006) Review of second-order models for adsorption system. *J Hazard Mater B* 136:681–689
45. Lagergren S (1898) Zur theorie der sogenannten adsorption geloster stoffe, *Kungliga Vetenska Vetenskapsakad. Handlingar* 24:1–39
46. Weber WJ, Morris JC (1963) Kinetics of adsorption on carbon from solution. *J Sanit Eng Div* 89:31–60
47. Anirudhan TS, Suchithra PS, Rijith S (2008) Amine-modified polyacrylamide– bentonite composite for the adsorption of humic acid in aqueous solutions. *Colloids Surf A* 326:147–156
48. Kleinedam S, Rugner H, Grathwohl P (1999) Impact of grain scale heterogeneity on slow sorption kinetics. *Environ Toxicol Chem* 18:1673–1678
49. Das BW, Mondal NK, Roy P, Chattaraj S (2013) Equilibrium, kinetic and thermodynamic study on Chromium(VI) removal from aqueous solution using *Pistia stratiotes* biomass. *Chem Sci Trans* 2:85–104